ACS APPLIED MATERIALS & INTERFACES

Research Article

www.acsami.org

Characterization of Free-Standing PEDOT:PSS/Iron Oxide Nanoparticle Composite Thin Films and Application As Conformable Humidity Sensors

Silvia Taccola,*[,†] Francesco Greco,[†] Alessandra Zucca,[†,‡] Claudia Innocenti,[§] César de Julián Fernández,[∥] Giulio Campo,[§] Claudio Sangregorio,[⊥] Barbara Mazzolai,[†] and Virgilio Mattoli*[,†]

[†]Center for Micro-BioRobotics @SSSA, Istituto Italiano di Tecnologia, Viale Rinaldo Piaggio 34 Pontedera, 56025 Italy

[‡]The Biorobotics Institute, Polo Sant'Anna Valdera, Scuola Superiore Sant'Anna, Viale Rinaldo Piaggio 34 Pontedera, 56025 Italy

[§]INSTM and Dipartimento di Chimica "U. Schiff", Università degli Studi di Firenze, via della Lastruccia 3-13, Sesto Fiorentino, I-50019 Firenze, Italy

[∥]C.N.R.−I.M.E.M Parco Area delle Scienze 37/A, I-43124 Parma, Italy

[⊥]C.N.R.−I.S.T.M. via C. Golgi 19, I-20133 Milano, Italy

Supporting Information

ABSTRACT: In this study, a new simple, fast, and inexpensive technique for the preparation of free-standing nanocomposite ultrathin films based on the conductive polymer poly(3,4-ethylenedioxythiophene):polystyrene sulfonate (PEDOT:PSS) and embedding iron oxide nanoparticles (NPs) is presented. These nanofilms were fabricated by a single step of spin-coated assisted deposition in conjunction with a release technique ("supporting layer technique") to detach them from the substrate. Free-standing nanofilms can be easily transferred onto several substrates due to their high conformability, preserving their functionalities. The effect of the addition of iron oxide nanoparticles on the structural and functional properties of the PEDOT:PSS nanofilms is investigated through topography, thickness, magnetic, magneto-optical activity, and conductivity characterizations. PEDOT:PSS and PEDOT:PSS/iron oxide NP nanofilms were tested as resistive humidity sensors. Their sensitivity to humidity was found to increase with increasing nanoparticle concentration. On the basis of these results, it is expected that these composites may furnish inexpensive and reliable means for relative humidity detection.

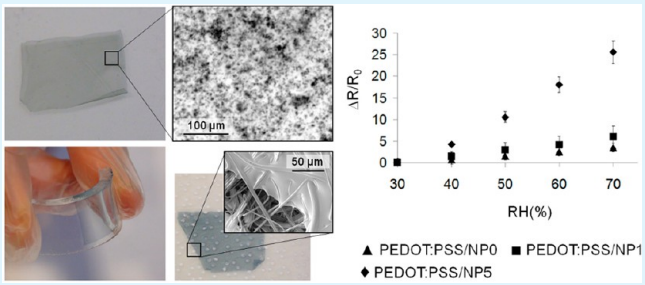

KEYWORDS: *PSS, iron oxide, nanocomposite, thin film, humidity sensor*

INTRODUCTION

In recent years, the development of nanocomposites containing inorganic materials and conducting polymers (e.g., polypyrrole, polyaniline, polythiophene, etc.) has drawn considerable attention because of their potential applications as light emitting diodes, photovoltaic solar cells, electromagnetic interference shields, microwave absorbing materials, magnetic recording media, supercapacitors, and sensors.[1−8] In particular, due to their low cost, ease of synthesis, room temperature operation, and high sensitivity, the conducting polymer-based nanocomposites have shown great potential as resistive-type sensors for gases (e.g., NH_3, H_2, CO) and humidity monitoring.[9−21] As an example, the response to exposure to different atmospheres was studied in composite polypyrrole thin films grown by chemical vapor deposition onto a granular metal film.[9,10]

To date, most of the literature focused on the composites made of polypyrrole (PPy) or polyaniline (PANI) and inorganic oxides (e.g., iron oxide, cobalt oxide, titanium oxide, etc.). Suri et al.[16] prepared PPy/Fe_2O_3 nanocomposites by a simultaneous gelation and polymerization process and studied their gas and humidity sensing properties. Parvatikar et al. synthesized PANI/WO_3,[17] PANI/Co_3O_4,[18] and PANI/CeO_2[19] composites by using chemical polymerization and investigated their humidity sensing properties. More recently, Su and co-workers synthesized TiO_2/PPy composite-based humidity sensors on alumina substrates[20] or on flexible PET substrates[21] by using an *in situ* photopolymerization route. Most of these inorganic/polymer composites sensors showed better sensing properties than pure polymers, such as higher sensitivity, quicker response, smaller hysteresis, and better stability.

Among conductive polymers, poly(3,4-ethylenedioxythiophene):polystyrene sulfonate (PEDOT:PSS) is very attractive

Received: April 15, 2013
Accepted: June 13, 2013
Published: June 13, 2013

because of its high conductivity, high work function, chemical stability, and transparency to visible light; in addition it is commercially available in the form of a ready-to-use waterborne dispersion. One of the main uses of PEDOT:PSS is in organic electronics: it acts as a hole transport layer in organic or polymer light-emitting diodes (OLEDs or PLEDs) because of its high work function, which can be optimized by various means, such as the incorporation of secondary doping agents.[22,23] Moreover, the PEDOT:PSS was reported as a water-absorbing material.[24] Such a property provides a basis for humidity-sensing applications. The influence of environmental relative humidity (RH) on the electrical and optical properties of PEDOT:PSS has been studied extensively by several researchers.[24−27] Kawano et al. reported the spatially inhomogeneous degradation of solar cell devices containing a PEDOT:PSS layer and ascribed this effect to water absorption causing the formation of insulating patches in PEDOT:PSS.[24] Similarly, Huang et al. reported the increase in resistivity of a PEDOT:PSS layer following its exposure to water.[25] A humidity and temperature sensor based on polyamide fibers coated with PEDOT:PSS was presented by Daoud et al., suggesting the development of sensing fabrics.[26] Quite recently, Liu et al. developed a humidity sensor based on PEDOT:PSS films and successfully demonstrated its application for detecting gravimetric water content in the soil.[27] However, to our knowledge, no attempts have been made to construct resistive-type humidity sensors based on PEDOT:PSS composite free-standing thin films.

Recently, a novel, fast, simple fabrication process for obtaining free-standing composite nanofilms composed of biodegradable polyesters (e.g., poly(*L*-lactic acid)) and superparamagnetic iron oxide nanoparticles was developed by our group.[28] The technique is based on a single step of spin-assisted deposition of a stable colloidal solution of the iron oxide nanoparticles and the polymer in a suitable solvent and a further release of the free-standing nanofilm in water by the dissolution of a sacrificial layer. These nanofilms can be manipulated and precisely positioned in liquid by using an external magnetic field and can thus provide a novel controllable support in biomedical applications.[28−30]

Herein, we propose to extend this method to conductive polymers for obtaining nanocomposite free-standing thin films of PEDOT:PSS embedding iron oxide nanoparticles (NPs). Large area free-standing conductive ultrathin films of PEDOT:PSS have been already successfully fabricated by our group.[31,32] The possibility to integrate iron oxide nanoparticles into the polymeric matrix allowed us to realize robust, flexible, conformable free-standing multifunctional PEDOT:PSS/iron oxide NP nanofilms retaining both magnetic and electrical conductivity functionalities.

Recently, a PEDOT:PSS/iron oxide NP nanocomposite was reported by Sun et al.[33] This composite, prepared by EDOT polymerization in the presence of an iron oxide NP ferrofluid, is in the form of a powder. The main advantage of the free-standing PEDOT:PSS/iron oxide NP composite nanofilms herein proposed lies in their easy transfer and adhesion onto several substrates with arbitrary shape and surface topography, preserving their functionality. The development and implementation of new sensing technologies on nonconventional substrates, such as flexible or stretchable substrates, have recently attracted increasing attention due to their applications in many different fields, for comfort, food and pharmaceutical quality and storage, safety, and security purposes.[34,35] Moreover, totally free-standing or partially anchored nanofilms (e.g., nanofilms suspended over microfabricated frames) or also those collected onto different solid substrates could be employed in a wide range of technological applications which demand materials exhibiting both electrical conductivity and magnetic properties.

Moreover, thanks to the electrical conductivity and the optical transparency of the polymer matrix, the conducting nanocomposite films can exhibit a magneto-optical activity. A magneto-optical technique has been already used for rewritable information storage media,[36] and more recently, the development of magneto-optical materials using nanoparticles has been receiving increasing interest for the development of optical magnetic field sensors[37−39] and in telecommunications for active optics.[40−42]

In this study, the morphological properties of PEDOT:PSS and PEDOT:PSS/iron oxide NP nanofilms were analyzed by atomic force microscopy (AFM) and scanning transmission electron microscopy (STEM). Furthermore, the electrical, magnetic, and magneto-optical properties of the nanofilms were investigated. Nanofilms have been studied as resistive sensors for the detection of relative humidity, and their sensitivity at different loadings of iron oxide NPs has been investigated.

EXPERIMENTAL SECTION

Fabrication of PEDOT:PSS and PEDOT:PSS/Iron Oxide NP Nanofilms. Free-standing composite PEDOT:PSS/iron oxide NP nanofilms and unloaded PEDOT:PSS nanofilms were obtained by spin-assisted deposition following the procedure described in detail elsewhere.[31] Briefly, silicon wafers (400-μm-thick, p-type, boron doped, ⟨100⟩, Si-Mat Silicon Materials) were cut (3 cm ×3 cm), cleaned for 10 min with a mixture of sulfuric acid and hydrogen peroxide (3:1), and then thoroughly rinsed with deionized water (DI) in order to remove dust and impurities. A thin film of poly(dimethylsiloxane) (PDMS, Sylgard 184 silicone elastomer base and curing agent, Dow Corning Corp.) was then deposited by spin-coating onto Si substrates. In order to obtain a thin elastomer film (thickness $t \approx 800$ nm), PDMS (10:1 ratio of base elastomer to curing agent) was diluted with *n*-hexane by 15% in weight. The diluted PDMS solution was spin-coated onto Si substrates for 150 s at a speed of 6000 rpm and then cured at $T = 95$ °C for 60 min in an oven. A subsequent air plasma treatment (Harrick PDC-002 Plasma Cleaner, HarrickPlasma) was applied with power $P = 5$ W for 30 s.

For neat PEDOT:PSS nanofilms (without iron oxide nanoparticles), a commercially available PEDOT:PSS aqueous dispersion (Clevios PH 1000, 1:2.5 PEDOT:PSS ratio, solid content 1.0 to 1.3%; Heraeus) was filtrated (Minisart, average pore size 1.20 μm, Sartorius) and then maintained at $T = 80$ °C until a reduction of 50% by weight was reached, caused by water evaporation. The concentrated PEDOT:PSS solution was then spin-coated over the cured PDMS film at 2000 rpm for 60 s. Then, samples underwent a thermal treatment (1 h; $T = 170$ °C). A 10% by weight poly(vinylalcohol) aqueous solution (PVA, average molecular weight $M_w = 30$ kDa, Sigma-Aldrich) was then drop cast over the samples and allowed to dry overnight forming the supporting layer. Sample edges were cut with a razor blade, and the bilayered film was carefully peeled off from the PDMS substrate with the aid of tweezers. The PEDOT:PSS free-standing nanofilm was finally released by dissolving the supporting PVA layer in DI water.

In order to incorporate the iron oxide NPs into the nanofilms, a commercially available water-based ferrofluid containing anionic coated superparamagnetic magnetite/maghemite nanoparticles (Fe_3O_4/γ-Fe_2O_3) having a nominal diameter of 10 nm (EMG 707, FerroTec Co.) was added to the concentrated dispersion of PEDOT:PSS and stirred with the aid of a vortex mixer for about 30 min. The resulting stable colloidal dispersion was used for film deposition by spin-coating, maintaining the same processes employed

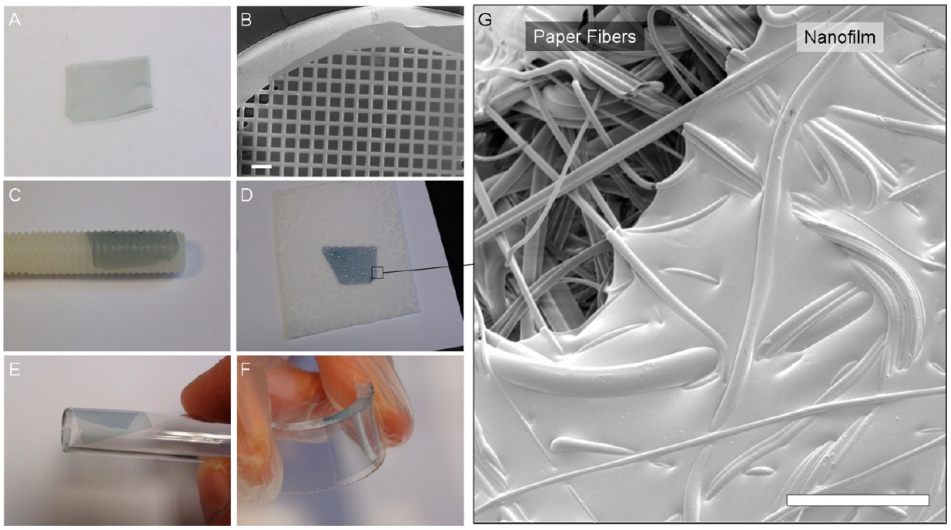

Figure 1. PEDOT:PSS/iron oxide NP composite nanofilms transferred to various substrates: (A) freestanding PEDOT:PSS/NP5 nanofilm (2 cm ×1 cm) floating in water after PVA dissolving. (B) SEM micrographs showing PEDOT:PSS/NP1 nanofilm collected onto a steel mesh (scale bar 100 μm). Nanofilms collected onto (C) Teflon screw, (D) paper, (E) plastic tube, and (F) flexible PDMS. In G, an SEM picture of the edge of a nanofilm collected on paper showing the paper fiber structure to which the nanofilm conforms (scale bar 50 μm).

for unloaded nanofilms. In this study, different nanofilms were prepared by varying the amount of magnetic fluid added to the solution. The samples were referred to as PEDOT:PSS/NP*x*, denoting films prepared using a colloidal solution with a concentration of *x* mg mL^{-1} iron oxide NPs (*x* = 0, 1, 5).

Morphological Properties. Nanofilms thickness, topography, and surface roughness were evaluated with a Veeco Innova Scanning Probe Microscope (Veeco Instruments Inc.) operating in tapping mode, using an RTESPA Al coated silicon probe (Veeco Instruments Inc.). All measurements were performed in the air, at room temperature, on films released in water and then collected and dried on a clean silicon wafer. For thickness measurements, SiO_2-supported nanofilms were scratched with a needle. Then from AFM topographic imaging across the edge of the scratch (scan range area 20 μm × 20 μm) it was possible to quantify the thickness, *t*, of the nanofilm, by measuring the height profile of the edge. For roughness measurements, the surface was scanned over 5 μm × 5 μm areas. Sample average roughness R_a and cross-section curves in the AFM images were obtained by software analysis (Gwyddion SPM analysis tool, http://gwyddion.net).

A microscopic investigation of the nanoparticle dispersion in the polymeric matrix of composite nanofilms was performed using scanning transmission electron microscopy (STEM) with a Helios NanoLab 600i Dual Beam (FEI Co.) operating at a 20.0 kV accelerating voltage. Specimens for STEM on nanofilm samples were prepared by collecting the free-standing nanofilms on regular copper TEM grids (SPI Inc.) and dried for 12 h in a desiccator prior to the STEM observation.

Magnetic Properties. The magnetic properties of the nanocomposite films were investigated using a Superconducting Quantum Interference Device Magnetometer (MPMS Quantum Design). The magnetization curves were recorded on dried films. The temperature dependences of the Zero-Field-Cooled (ZFC) and Field-Cooled (FC) magnetizations were recorded using a magnetic field of 50 Oe, after cooling the sample in the presence (FC) or in the absence (ZFC) of the magnetic field. The hysteresis loops were measured at 2.5 K and at 300 K by cyclically applying a magnetic field up to ±50 kOe.

Magneto-Optical Measurements. Magneto-optical spectra were measured at room temperature using a homemade setup. The magnetic circular dichroism (MCD) spectra were recorded in the nUV−vis−nIR range from 300 to 800 nm applying a magnetic field of 12.5 kOe. The dichroism, i.e. the variation of intensity of the transmitted light obtained by changing the polarization from left- to right-hand, was measured using a photomultiplier (Hamamatsu, model R376 head on). In this measurement, the magnetic field and the wavevector of the light were parallel and both perpendicular to the surface of the film. MO hysteresis loops were also recorded at fixed wavelengths.

Electrical Properties. Sheet resistance of the obtained films was evaluated by using a homemade four probe apparatus. A four probe head (JANDEL Engineering Ltd.) equipped with four retractable tungsten carbide tips was mounted on an *x*, *y*, *z*, θ manual micropositioning system (Melles Griot). The two external tips were connected to a galvanostat (Mod. 7050, AMEL) that permitted the controlled flow of a i = 1 μA current. The two internal tips were connected to a voltmeter, measuring the voltage *V*. Sheet resistance, Rs, of the nanofilm samples was measured, and the related conductivity, σ, has been calculated making use of formulas: $Rs = \pi/\ln 2\ (V/i)$; $\sigma = 1/(Rs\ t)$ where *t* was the nanofilm thickness as determined by AFM measurements. Sheet resistance of the nanofilms was measured prior to their release in water.

Humidity Sensing Properties. For humidity sensing studies, free-standing nanofilms have been transferred onto a solid support made of polystyrene, cut from a polystyrene sheet using a laser cutter (Versalaser, Universal Laser Systems). A pair of gold metal electrodes with a thickness of 200 nm was deposited on the polystyrene substrates by DC sputtering in a high vacuum sputter system (Q150T S Turbo-Pumped Sputter Coater, Quorum Technologies Ltd.). PEDOT:PSS and PEDOT:PSS/NP*x* nanofilms were then collected from the suspended state onto the polystyrene substrates and dried for 12 h in a desiccator. The samples were placed in a climatic test chamber (CTC 256, Memmert) with humidity and temperature control. The samples were externally wired for the connection to a data acquisition card (USB-6216 DAQ device, National Instruments) controlled by the LabVIEW SignalExpress software package. The DC electrical resistance of the samples was measured at an applied voltage of 5 V, at a constant temperature of 30 °C, and various humidity levels from 30 to 70% RH (with humidity intervals of 10% RH). The relative humidity inside the chamber was monitored by a standard precalibrated humidity meter. Moreover, the response of the nanofilms to a change in temperature was measured between 20 and 50 °C (with temperature intervals of 10 °C) at a constant relative humidity of 50%. For each nanoparticle concentration, measurements were carried out on 10 different samples.

RESULTS AND DISCUSSION

Microstructure Characteristics of PEDOT:PSS and Composite Nanofilms. PEDOT:PSS and PEDOT:PSS/iron

dx.doi.org/10.1021/am4013775 | ACS Appl. Mater. Interfaces 2013, 5, 6324−6332

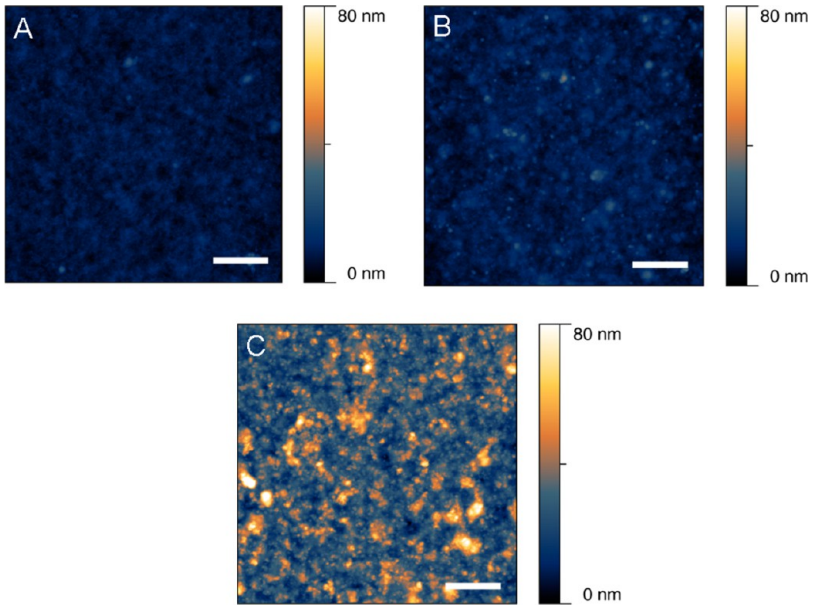

Figure 2. Atomic force microscope scans of nanofilms with increasing NP concentration: (A) PEDOT:PSS/NP0; (B) PEDOT:PSS/NP1; (C) PEDOT:PSS/NP5 (scale bar 1 μm). The formation of clusters is observed as the concentration of nanoparticles increases, corresponding to the increase of the surface roughness value, as reported in Table 1.

oxide NP composite nanofilms were released from the peeled bilayered film after immersion in deionized water by the dissolution of the PVA supporting layer (Figure 1A). The resulting free-standing nanofilms could be easily manipulated in water with metal tweezers or pipettes, folded and unfolded multiple times without breaking. The flexibility and the robustness of the PEDOT:PSS nanofilms, already tested for unloaded films,[31] were thus maintained in the case of nanocomposite films. Moreover, nanofilms containing iron oxide NPs could be displaced in water by using a permanent magnet. A movie of magnetic nanofilm manipulation is available in the Supporting Information. From the freely suspended state, the films could be easily transferred onto rigid substrates such as Si, steel, and glass, as well as onto compliant ones, e.g., elastomers, paper, or also on plastic frames and metal meshes with arbitrary shapes and topographies, without suffering from damage or ruptures (Figure 1B–G). Thanks to the nanometric thickness, these nanofilms adhered firmly to the substrates and showed good conformability to flat or irregular surfaces. The use of a magnet could facilitate nanofilm handling during the transfer procedure (see Supporting Information movie).

AFM surface analysis was performed for each sample to investigate nanofilms' surface topology and particle dispersion in the nanocomposite. Flat, homogeneous surface topography was observed by AFM in nonmagnetic nanofilms (Figure 2A). In samples containing iron oxide NPs, the presence of clusters emerging from the surface of the samples was evident (Figure 2B,C).

Grains observed in AFM micrographs were confirmed to be iron oxide NP clusters by STEM analysis. Bright-field STEM micrographs showed the presence of iron oxide nanoparticle clusters (dark spots) uniformly distributed within the polymeric matrix (bright; Figure 3A,C). Moreover, the presence of individual nanoparticles could be clearly distinguished (Figure 3B,D).

Due to particle clustering, the surface microroughness (R_a) increased with the amount of iron oxide NPs in the nanocomposite (Table 1). The incorporation of iron oxide NPs also affected the thickness of the nanofilms. As reported in Table 1, the average thickness increased with respect to the amount of magnetic nanoparticles added to the solution. The phenomenon of nanoparticle clustering and the increase of surface roughness and thickness with respect to the amount of nanoparticles embedded in the structure have been also evidenced in our previous study concerning nanocomposite nanofilms composed of polyester.[28]

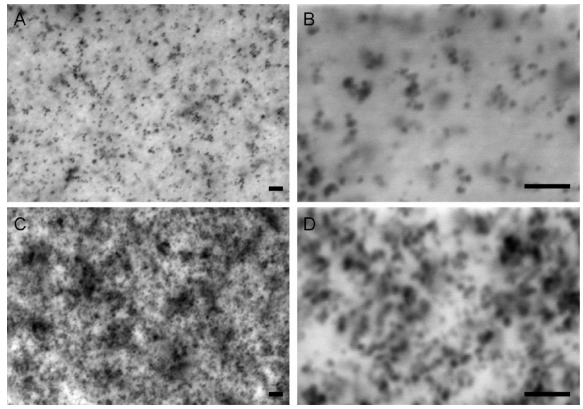

Figure 3. STEM micrographs of nanocomposite PEDOT:PSS nanofilms: (A, B) PEDOT:PSS/NP1; (C, D) PEDOT:PSS/NP5 (scale bar 100 nm).

Table 1. Roughness (R_a), Thickness (t), and Conductivity (σ) of PEDOT:PSS and PEDOT:PSS/NP*x* Nanofilms

sample	R_a (nm)	t (nm)	σ (S cm^{-1})
PEDOT:PSS/NP0	1.5	218 ± 13	1.96 ± 0.14
PEDOT:PSS/NP1	3.1	231 ± 15	0.92 ± 0.10
PEDOT:PSS/NP5	8.5	269 ± 19	0.38 ± 0.06

Magnetic Properties of Composite Nanofilms. The magnetic properties of the composite nanofilms were

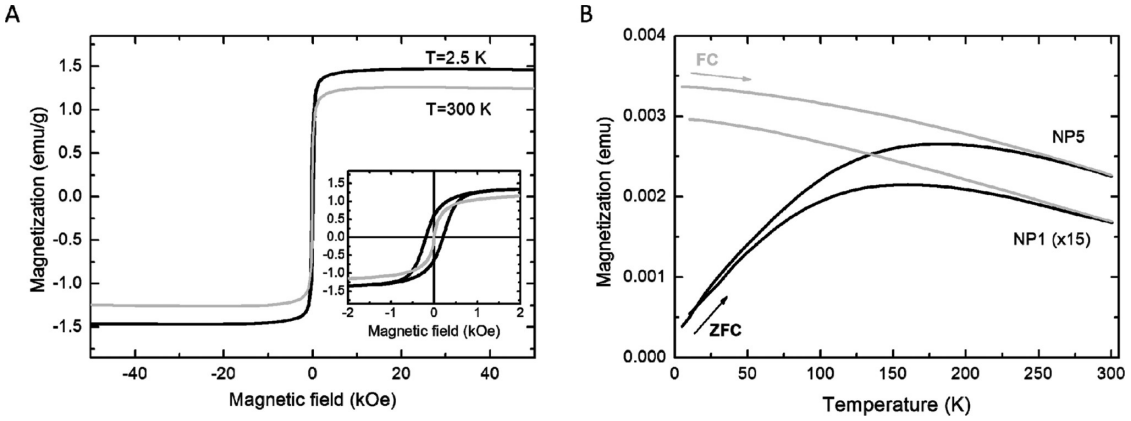

Figure 4. (A) Magnetic field dependence of the magnetization for PEDOT:PSS/NP5 at low (2.5 K) and high (300 K) temperature. The inset shows a magnification of the hysteresis loops. (B) Temperature dependence of the ZFC-FC magnetizations of PEDOT:PSS/NP1 and PEDOT:PSS/NP5 nanofilms.

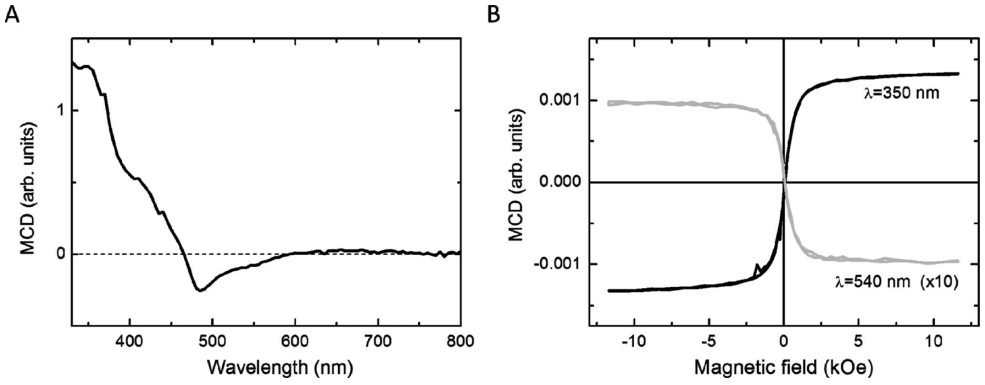

Figure 5. Magneto-optical properties of the PEDOT:PSS/NP5 nanofilm measured at room temperature. (A) MO spectrum; (B) MCD hysteresis loops measured at two different wavelengths.

investigated by measuring the field and temperature dependence of the magnetization. Figure 4A displays the hysteresis loops of PEDOT:PSS/NP5 measured at 2.5 and 300 K. At low temperatures, the loop is open with a coercive field, H_C = 200 Oe, a reduced remanence M_{0T}/M_{5T} = 0.46, and a saturation magnetization M_S = 1.46 emu/g. Conversely, at room temperature no hysteresis is observed, suggesting all the particles are in the superparamagnetic regime. The observed behavior strictly resembles that measured for the aqueous solution of the magnetite nanoparticles alone (Figure S1, Supporting Information), indicating that the magnetic properties of the pristine ferrofluid were successfully transferred to the film without significant modification.

PEDOT:PSS/NP1 nanocomposite exhibits a very similar behavior (H_C = 200 Oe, M_{0T}/M_{5T} = 0.41) with a magnetization of saturation of 0.18 emu/g (Figure S2, Supporting Information). The M_S ratio of the two nanocomposites, which is proportional to the amount of magnetic component occurring in the film, is ca. 8, larger than the nominal concentration ratio, which is 5. This discrepancy can be ascribed to the precipitation of larger nanoparticle aggregates during the spin coating process for PEDOT:PSS/NP5 samples.

Interestingly, however, repeating the same measurement on different pieces of the nanocomposites always afforded reproducible results, thus providing evidence of a homogeneous distribution of the nanoparticles within the film.

The room temperature superparamagnetism of the system was confirmed by ZFC-FC magnetization measurements (Figure 4B). In fact, the average blocking temperature, T_B, which is identified with the temperature of the maximum of the ZFC curve, is well below room temperature for both samples. This means that the nanocomposites present a nonzero magnetization only when exposed to an external magnetic field. Therefore the samples are normally nonmagnetic but preserve the capability to respond to an external magnetic stimulus.

The shape of the two ZFC-FC curves of the two nanocomposites are similar apart from a shift of T_B, which is larger for PEDOT:PSS/NP5 (183 K) than for PEDOT:PSS/NP1 (158 K). This difference can be ascribed to the effect of magnetic dipolar interparticle interactions which are expected to be stronger on the most concentrated nanocomposite. Indeed, STEM micrographs (Figure 3) show the occurrence of larger nanoparticle aggregates, in size and number in PEDOT:PSS/NP5.

Magneto-Optical Properties of Composite Nanofilms. In order to get better insight on the stability of the inorganic component of the composites during the embedding process, we investigated the magneto-optical properties of PEDOT:PSS/NP5 at room temperature as a function of the wavelength and of the magnetic field. Indeed, the possible oxidation of the metastable magnetite phase (Fe_3O_4, Fe(II,III) oxide) to maghemite (γ-Fe_2O_3, Fe(III) oxide) can be relevant for the physical properties of the final product since the two iron oxides have different conductivities.[43] On the other hand, magnetic measurements do not allow for discriminating

between magnetite and maghemite since the two oxides have similar magnetic properties.

The MCD spectrum (Figure 5A) exhibits a structured line shape that can be related to the electronic transitions of an iron oxide spinel. The comparison with literature data[44−46] allows for assigning the spectral features observed below 400 nm to electronic charge transfer transitions of Fe^{3+} ions in octahedral sites of a spinel lattice and the line shape between 400 and 550 nm to double crystal field transitions of Fe^{3+} of the maghemite. This observation, together with the absence of the broad negative band at ca. 600−700 nm of Fe^{2+} in octahedral sites, indicates the magnetic phase is mainly maghemite.

This conclusion is corroborated by the analysis of the MO hysteresis loops recorded at different wavelengths (Figure 5B). Since at 350 and 540 nm maghemite and magnetite contribute differently to the total magneto-optical signal, the presence of both phases would result in a modification of the loop shape, which, on the contrary, is not the case here.

Electrical Properties of PEDOT:PSS and Composite Nanofilms. One of the major limitations for nanocomposite materials containing conductive polymer and magnetic nanoparticles is the electrical conductivity that is often rather poor.[1] In order to evaluate the effect of the inclusion of the iron oxide NPs on nanofilm conductivity, σ, the electrical properties of the proposed nanofilms have been investigated. The measurements enabled us to compare the different electrical properties of the films prepared with different amount of nanoparticles. The obtained values of conductivity σ for the different types of nanofilms are displayed in Table 1. Maximum conductivity was found for unloaded samples (σ = 1.96 ± 0.14 S cm^{-1}) as expected. The result is in good agreement with those already reported by our group on similar PEDOT:PSS nanofilms having a slightly lower thickness.[31] For composite nanofilms, the conductivity decreased with increasing the iron oxide NP content. The decreased conductivity of the nanofilms in the presence of magnetic nanoparticles is ascribable to the insulating properties of iron oxide nanoparticles (consisting mainly of the maghemite phase) and to the partial blockage of the conduction path between PEDOT-rich domains by the nanoparticles embedded in the PEDOT:PSS matrix.[47] Although the presence of iron oxide NPs led to a decrease in the conductivity of composite nanofilms, its value is still relatively high even at the maximum studied loading (i.e., PEDOT:PSS/NP5, σ = 0.38 ± 0.06), thus permitting their practical use as resistive sensors.

Humidity and Temperature Sensitivity of PEDOT:PSS and Composite Nanofilms. As described in the Experimental Section, humidity sensing studies were carried out on PEDOT:PSS/NP*x* nanofilms that were collected and dried onto polystyrene substrate frames (Figure 6A). The geometry of substrates and suspended nanofilms employed in these experiments is shown in Figure 6B.

The response of the nanofilms to humidity was investigated in the range of 30−70% RH. This humidity range was selected because previous studies on PEDOT:PSS as a humidity sensing material evidenced that the resistivity of PEDOT:PSS thin films deposited by drop casting on a glass substrate increased linearly up to 80% RH and then decreased dramatically above that value.[48] This behavior, ascribed to water droplet formation on the surface of the films at high RH, was evidenced also by the authors in a preliminary set of experiments performed on PEDOT:PSS/NP*x* nanofilms over a wider range of relative humidity (30−90% RH; data not shown).

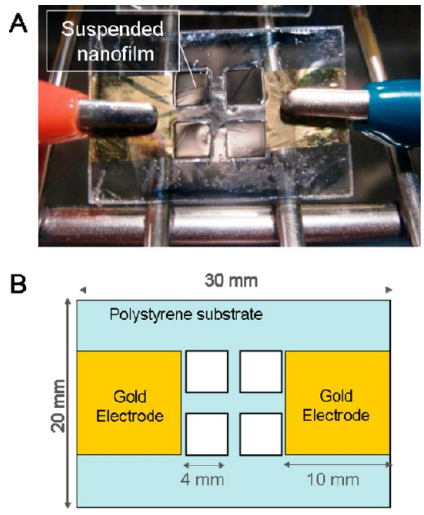

Figure 6. (A) A picture and (B) the structure of the samples used for humidity sensing studies.

The results from humidity-sensing experiments showed that, in the range of 30−70% RH, the resistance of PEDOT:PSS/NP*x* nanofilms linearly increased when exposed to increasing levels of relative humidity, consistent with previous observations.[27,48] Figure 7A shows the change in resistance ($\Delta R/R_0$ (%) with $\Delta R = R - R_0$ and R_0 the value of resistance measured at 30% RH) with respect to environmental relative humidity RH for nanofilms having different concentrations of iron oxide NPs.

As regards unloaded nanofilms made of PEDOT:PSS, it is known that the resistivity of the PEDOT:PSS increases as RH increases.[25,27,47] This behavior is due to the microscopic structure of PEDOT:PSS films realized starting from aqueous dispersions that are characterized by a granular structure in which PEDOT-rich grains (conductive) are surrounded by PSS (insulator, hydrophilic). Such a granular structure was evidenced in many studies devoted to elucidating PEDOT:PSS thin film microstructures by employing X-ray photoelectron spectroscopy (XPS), STEM-EDX, and AFM.[49−52] The size of PEDOT-rich grains is typically some tens of nanometers, and it varies among different commercially available PEDOT:PSS aqueous dispersions, depending on the relative ratio between PEDOT and PSS. In the case of the material employed in this study, the size of the grains is on the order of ∼30 nm.[31,52] Grain size distribution and connectivity between grains strongly affect the actual conductivity of the films, as in many other organic conductors based on hopping mechanism. The number and height of hopping barriers is critically related to the amount and arrangement of the long PSS chains to which partially oxidized PEDOT smaller chains are interlinked. Many different parameters, including thermal treatments and environmental moisture, as well as the introduction of dopants, can affect the nanoscale morphology of this granular structure, thus leading to different conductivity.[25] In the case of water uptake from environmental moisture, the observed decrease in conductivity is typically ascribed to decreasing electrical interconnections between PEDOT chains as a result of swelling of the polymer (PSS) by the water uptake.[53] Moreover, since dipole moments of doping molecules can influence the conductivity of polymers, the conductivity of PEDOT:PSS may decrease also due to the strong dipole moment of water molecule acting as a screening agent between the conductive sites located in the PEDOT-rich

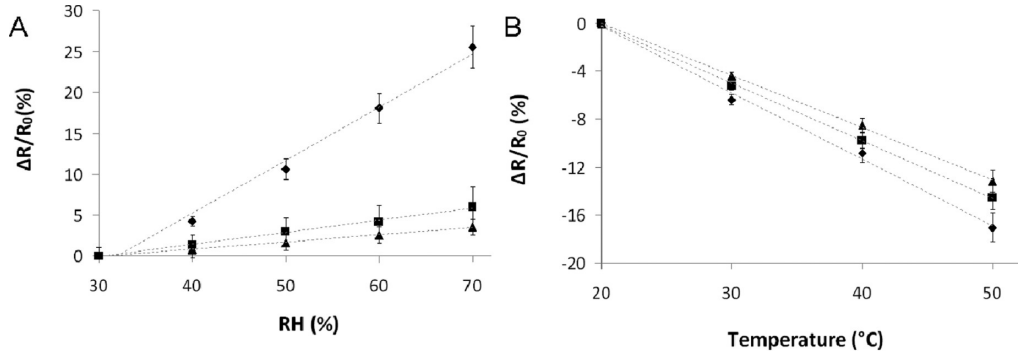

Figure 7. The change in the resistance of PEDOT:PSS and PEDOT:PSS/NP*x* nanofilms versus (A) relative humidity and (B) temperature for different NP concentrations: x = 0 (▲); 1 (■); 5 (♦) mg mL^{-1}.

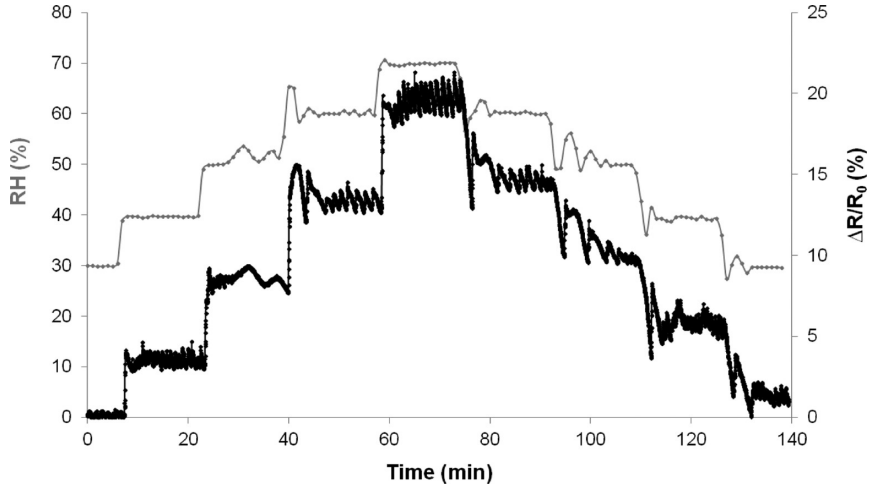

Figure 8. The change in the resistance (black curve) of a PEDOT:PSS/NP5 nanofilm during humidity step-change experiments (gray curve) in the range of 30−70% RH.

regions.[54] Furthermore, the great increase of conductivity above 80% RH mentioned above has been attributed to the formation of a water meniscus layer on the water-saturated polymer films, which dissolves PSS protons and also some atmospheric gases (e.g., O_2 and CO_2) and leads to an ionic conductivity.[48] Then PEDOT:PSS devices are stable and sensitive to the moisture as humidity sensors below a humidity level around 80% RH.

As regards composite nanofilms with different concentrations of iron oxide NPs, it can be seen in Figure 7A that they showed enhanced sensitivity (S) to moisture, defined as $S = (\Delta R/R_0\ (\%))/\Delta\mathrm{RH}(\%)$, with respect to nanofilms made of PEDOT:PSS only. Both the samples PEDOT:PSS/NP1 and PEDOT:PSS/NP5 showed a linear response with respect to RH, while the maximum total percentage change in resistance was observed for the PEDOT:PSS/NP5 sample (25% for a 30−70% change in relative humidity, corresponding to a sensitivity S of about 0.65, to be compared with 0.15 and 0.09 of, respectively, PEDOT:PSS/NP1 and PEDOT:PSS samples). The observed effect of enhancement of sensitivity in composite sensors is ascribable to the differences in the nanostructure of the nanofilms. As already mentioned, the insertion of iron oxide NPs with a nominal diameter of 10 nm largely modified the morphology and surface roughness of nanofilms. The increased roughness accounts for a larger exposed surface for the composite nanofilms with respect to the purely polymeric ones. Because of the known effect of partial phase segregation between PEDOT and PSS due to the thermal treatment[25] and because of the enrichment in PSS observed at film surfaces,[55] much more PSS could be exposed on the surface of composite nanofilms, thus increasing the water sorption from environmental moisture. Moreover, because of the comparable size between NPs and PEDOT domains, the introduction of NPs could cause a relevant change in the PEDOT-interparticle arrangement with a much more disordered organization, by modifying distances between PEDOT-rich grains and by increasing the number of PEDOT/PSS/PEDOT or PEDOT/PSS/NPs interfaces. Interesting effects on film structure and particle reorganization have been observed for example in the case of PEDOT:PSS/ZnO nanoparticle composites, in which the presence of NPs induced a change of the chemical structure of the polymer and a conformational change of the PEDOT polymer chains. Such modifications had relevant consequences on the material conductivity.[56]

As visible in Figure 8, the response of the samples to subsequent steps of increasing and decreasing relative humidity is very good and stable, with the resistance of the sensor returning almost to the initial value after a complete series of tests in the range of 30−70% RH was completed. The sensor response to the change in humidity was very fast, with a response time of around 1 s. It is interesting to notice that the sensor was able to follow even the small and fast oscillations of relative humidity around the set value, due to the climatic chamber trying to reach stability. From the graph in Figure 8, it is also possible to preliminarily appreciate the relatively low

hysteresis of the system, which can be estimated around 3% RH. In order to further characterize the performances of the film as a humidity sensor, noise tests have been carried out in an isolated environment. From these tests, we estimated the noise on the order of 0.01% RH (as RMS value). The measurements have been performed with a resolution of about 0.005% RH (16 bit ADC resolution). These values make it possible to detect a humidity variation on the order of 0.03−0.05% RH, even better than commercial high-quality low-cost humidity sensors (such as for example the Sensirion SHT11, www.sensirion.com), paving the way for a possible real world application of the proposed technology.

Along with the characterization of moisture sensitivity, sensor samples were also subjected to variations in the surrounding temperature between 20 and 50 °C, in order to test their response. Figure 7B shows the change in resistance ($\Delta R/R_0$(%), R_0 value taken at 20 °C) with respect to temperature for nanocomposites having different concentrations of iron oxide NPs. It can be observed that the resistance clearly decreased with increasing temperature, as typically observed in disordered semiconductors. Typical thermal drift for the sensors is on the order of 0.5 $\Delta R/R_0$ (%)/°C, slightly depending on the composition.

In order to demonstrate the feasibility of the proposed system for developing conformable humidity sensors that could be deployed on various surfaces of interest, additional tests were carried out studying the humidity sensing behavior of PEDOT:PSS/NP5 nanofilms collected onto rectangular glass slides (20 mm × 30 mm) and small paper stripes (20 mm × 30 mm) with complex surface topography (showed in Figure 1G). No difference in the humidity response of the nanofilms was observed, confirming the independence of the response from the substrate (Figure S3, Supporting Information).

CONCLUSIONS

Fabrication of multifunctional nanocomposite thin films from PEDOT:PSS and iron oxide nanoparticles was obtained by employing an effective, simple, and fast single-step process. The amount of iron oxide nanoparticles strongly affects the resulting nanofilms, influencing their morphological, conductive, and magnetic properties, while preserving their integrity, manipulability, and conformability when released as free-standing nanofilms. PEDOT:PSS/iron oxide nanoparticle composites showed better humidity sensing as compared to PEDOT:PSS only, when tested both in the form of suspended nanofilm membranes and of nanofilms collected on solid substrates. The sensitivity was found to increase with increasing nanoparticle concentration. This work could lead to the development of simple and reliable conformable humidity sensors easily transferrable onto several rigid and flexible substrates with arbitrary shape and surface topography. Moreover, successful incorporation of iron oxide nanoparticles into conductive polymer matrices opens up perspectives for their utilization in the fields of electronics, telecommunications, and optics.

ASSOCIATED CONTENT

Supporting Information

A movie showing the manipulation of PEDOT:PSS/iron oxide NP composite nanofilms in water by using a permanent magnet. Three additional figures showing the low temperature magnetic hysteresis properties of the employed ferrofluid (Figure S1) and composite nanofilms (Figure S2) and the humidity sensing behavior of PEDOT:PSS/NP5 nanofilms collected onto glass and paper substrates (Figure S3). This information is available free of charge via the Internet at http://pubs.acs.org.

AUTHOR INFORMATION

Corresponding Author

*Tel.: +39 050 883417. Fax: +39 050 883402. E-mail: silvia.taccola@iit.it; virgilio.mattoli@iit.it.

Author Contributions

The manuscript was written through contributions of all authors. All authors have given approval to the final version of the manuscript.

Notes

The authors declare no competing financial interest.

REFERENCES

(1) Gangopadhyay, R.; De, A. *Chem. Mater.* **2000**, *12*, 608−622.
(2) Sanchez, C.; Julián, B.; Belleville, P.; Popall, M. *J. Mater. Chem.* **2005**, *15*, 3559−3592.
(3) Novak, B. M. *Adv. Mater.* **1993**, *5*, 422−433.
(4) Wang, G. F.; Tao, X. M.; Wang, R. X. *Nanotechnology* **2008**, *19*, 145201−145206.
(5) Beek, W. J. E.; Wienk, M. M.; Janssen, R.A. J. *Adv. Mater.* **2004**, *16*, 1009−1013.
(6) Gómez, H.; Ram, M. K.; Alvi, F.; Villalba, P.; Stefanakos, E.; Kumar, A. *J. Power Sources* **2011**, *196*, 4102−4108.
(7) Makeiff, D. A.; Huber, T. *Synth. Met.* **2006**, *156*, 497−505.
(8) Gass, J.; Poddar, P.; Almand, J.; Srinath, S.; Srikanth, H. *Adv. Funct. Mater.* **2006**, *16*, 71−75.
(9) Bruschi, P.; Cacialli, F.; Nannini, A. *Sens. Actuators, A* **1992**, *32*, 313−317.
(10) Bruschi, P.; Cacialli, F.; Nannini, A.; Neri, B. *Sens. Actuators, B* **1994**, *19*, 421−425.
(11) Gangopadhyay, R.; De, A. In *Handbook of Organic−Inorganic Hybrid Materials and Nanocomposites*; Nalwa, H. S., Eds.; American Scientific Publishers: Valencia, CA, 2003; Vol. 2, p 217.
(12) Gangopadhyay, R.; De, A. *Sens. Actuators, B* **2001**, *77*, 326−329.
(13) Ram, M. K.; Yavuz, Ö.; Lahsangah, V.; Aldissi, M. *Sens. Actuators, B* **2005**, *106*, 750−757.
(14) Ram, M. K.; Yavuz, Ö.; Aldissi, M. *Synth. Met.* **2005**, *151*, 77−84.
(15) Tandon, R. P.; Tripathy, M. R.; Arora, A. K.; Hotchandani, S. *Sens. Actuators, B* **2006**, *114*, 768−773.
(16) Suri, K.; Annapoorni, S.; Sarkar, A. K.; Tandon, R. P. *Sens. Actuators, B* **2002**, *81*, 277−282.
(17) Parvatikar, N.; Jain, S.; Khasim, S.; Revansiddappa, M.; Bhoraskar, S. V.; Ambika Prasad, M. V. N. *Sens. Actuators, B* **2006**, *114*, 599−603.
(18) Parvatikar, N.; Jain, S.; Kanamadi, C. M.; Chougule, B. K.; Bhoraskar, S. V.; Prasad, M. V. N. A. *J. Appl. Polym. Sci.* **2007**, *103*, 653−658.
(19) Parvatikar, N.; Jain, S.; Bhoraskar, S. V.; Prasad, M. V. N. A. *J. Appl. Polym. Sci.* **2006**, *102*, 5533−5537.
(20) Su, P. G.; Huang, L. N. *Sens. Actuators, B* **2007**, *123*, 501−507.
(21) Su, P. G.; Wang, C. P. *Sens. Actuators, B* **2008**, *129*, 538−543.
(22) Brown, T. M.; Cacialli, F. *J. Polym. Sci., Part B: Polym. Phys.* **2003**, *41*, 2649−2664.
(23) Nardes, A. M.; Kemerink, M.; de Kok, M. M.; Vinken, E.; Maturova, K.; Janssen, R. A. *Org. Electron.* **2008**, *9*, 727−734.
(24) Kawano, K.; Pacios, R.; Poplavskyy, D.; Nelson, J.; Bradley, D. D. C.; Durrant, J. R. *Sol. Energy Mater. Sol. Cells* **2006**, *90*, 3520−3530.
(25) Huang, J.; Miller, P. F.; Wilson, J. S.; de Mello, A. J.; de Mello, J. C.; Bradley, D. D. C. *Adv. Funct. Mater.* **2005**, *15*, 290−296.
(26) Daoud, W. A.; Xin, J. H.; Szeto, Y. S. *Sens. Actuators, B* **2005**, *109*, 329−333.
(27) Liu, J.; Agarwal, M.; Varahramyan, K.; Berney, E. S., IV; Hodo, W. D. *Sens. Actuators, B* **2008**, *129*, 599−604.

(28) Taccola, S.; Desii, A.; Pensabene, V.; Fujie, T.; Saito, A.; Takeoka, S.; Dario, P.; Menciassi, A.; Mattoli, V. *Langmuir* **2011**, *27*, 5589−5595.
(29) Pensabene, V.; Mattoli, V.; Fujie, T.; Menciassi, A.; Takeoka, S.; Dario, P. *IEEE Nano Proc.* **2009**, 403−407.
(30) Mattoli, V.; Sinibaldi, E.; Pensabene, V.; Taccola, S.; Menciassi, A.; Dario, P. *ICRA Proc.* **2010**, 1604−1609.
(31) Greco, F.; Zucca, A.; Taccola, S.; Menciassi, A.; Fujie, T.; Haniuda, H.; Takeoka, S.; Dario, P.; Mattoli, V. *Soft Matter* **2011**, *7*, 10642−10650.
(32) Greco, F.; Zucca, A.; Taccola, S.; Menciassi, A.; Dario, P.; Mattoli, V. *MRS Proc.* **2012**, *1403*, 1−6.
(33) Sun, D. C.; Sun, D. S. *Mater. Chem. Phys.* **2009**, *118*, 288−292.
(34) Wang, X.; Larsson, O.; Platt, D.; Nordlinder, S.; Engquist, I.; Berggren, M.; Crispin, X. *Sens. Actuators, B* **2012**, *166−167*, 556−561.
(35) Briand, D.; Oprea, A.; Courbat, J.; Bârsan, N. *Mater. Today* **2011**, *14*, 416−423.
(36) Mansuripur, M. *J. Phys. D: Appl. Phys.* **2001**, *34*, 87−102.
(37) Martinez, L.; Cecelja, F.; Rakowski, R. *Sens. Actuators, A* **2005**, *123−124*, 438−443.
(38) Zayat, M.; Pardo, R.; Rosa, G.; del Real, R. P.; Diaz-Michelena, M.; Arruego, I.; Guerrero, H.; Levy, D. *J. Sol-Gel Sci. Technol.* **2009**, *50*, 254−259.
(39) Sun, L.; Jiang, S.; Marciante, J. R. *Opt. Express* **2010**, *18*, 5407−5412.
(40) Levy, M. *IEEE J. Sel. Top. Quant. Electron.* **2002**, *8*, 1300−1306.
(41) Hutchings, D. C. *J. Phys. D: Appl. Phys.* **2003**, *36*, 2222−2229.
(42) Kahl, S.; Grishin, A. M. *Appl. Phys. Lett.* **2004**, *84*, 1438−1440.
(43) Cornell, R. M.; Schwertmann, U. In *The Iron Oxides: Structure, Properties, Reactions, Occurences and Uses*, 2nd ed.; Wiley-VCH Verlag: Weinheim, Germany, 1996; Chapter 6, p 115.
(44) Fontijn, W. F. J.; van der Zaag, P. J.; Devillers, M. A. C.; Brabers, V. A. M.; Metselaar, R. *Phys. Rev. B* **1997**, *56*, 5432−5442.
(45) Kim, K. J.; Lee, H. S.; Lee, M. H.; Ho Lee, S. *J. Appl. Phys.* **2002**, *91*, 9974−9977.
(46) He, Y. P.; Miao, Y. M.; Li, C. R.; Wang, S. Q.; Cao, L.; Xie, S. S.; Yang, G. Z.; Zou, B. S.; Burda, C. *Phys. Rev. B* **2005**, *71*, 125411−125419.
(47) Guo, Z.; Shin, K.; Karki, A. B.; Young, D. P.; Kaner, R. B.; Hahn, H. T. *J. Nanopart. Res.* **2009**, *11*, 1441−1452.
(48) Kus, M.; Okur, S. *Sens. Actuators, B* **2009**, *143*, 177−181.
(49) Greczynski, G.; Kugler, T.; Salaneck, W. R. *Thin Solid Films* **1999**, *354*, 129.
(50) Nardes, A. M.; Kemerink, M.; Janssen, R. A. J.; Bastiaansen, J. A. M.; Kiggen, N. M. M.; Langeveld, B. M. W.; van Breemen, A. J. J. M.; de Kok, M. M. *Adv. Mater.* **2007**, *19*, 1196−1200.
(51) Nardes, A. M.; Janssen, R. A. J.; Kemerink, M. *Adv. Funct. Mater.* **2008**, *18*, 865−871.
(52) Yan, H.; Arima, S.; Mori, Y.; Kagata, T.; Sato, H.; Okuzaki, H. *Thin Solid Films* **2009**, *517*, 3299−3303.
(53) Crispin, X.; Marciniak, S.; Osikowicz, W.; Zotti, G.; Denier Van Der Gon, A. W.; Louwet, F.; Fahlman, M.; Groenendaal, L.; De Schryver, F.; Salaneck, W. R. *J. Polym. Sci. Part B* **2003**, *41*, 2561−2583.
(54) Borsenberger, P. M.; Bassler, H. *J. Chem. Phys.* **1991**, *95*, 5327−5331.
(55) Greczynski, G.; Kugler, T.; Keil, M.; Osikowicz, W.; Fahlman, M.; Salaneck, W. R. *J. Electron Spectrosc. Relat. Phenom.* **2001**, *121*, 1−17.
(56) Semaltianos, N. G.; Logothetidis, S.; Hastas, N.; Perrie, W.; Romani, S.; Potter, R. J.; Dearden, G.; Watkins, K. G.; French, P.; Sharpet, M. *Chem. Phys. Lett.* **2010**, *484*, 283−289.